

Structural, surface morphological, optical and electrical properties of In_xSe_y thin films, an absorber layer for photovoltaic cells fabricated by M-CBD method using different variables

Fatih ÜNAL^{1*}, Serkan DEMİR², Hasan MAMMADOV³

¹Giresun University, Central Research Laboratory, Application and Research Center, Giresun, Turkey

²Department of Industrial Engineering, Faculty of Engineering, Giresun University, Giresun, Turkey

³Department of Physics, Faculty of Arts and Sciences, Kafkas University, Kars, Turkey

Received: 01.04.2021 • Accepted/Published Online: 22.06.2021 • Final Version: 20.12.2021

Abstract: Mixed-phased In_xSe_y thin film containing InSe, In_2Se_3 and In_6Se_7 phases was prepared by M-CBD method and characterized by X-ray diffraction, AFM, optical spectroscopy and J-V measurements. Structural, optical and electrical conductance properties were modified by annealing the films at different temperatures. Optical and morphological properties were also investigated dependently on temperature and concentration of cationic precursor solution. It has been observed with annealing that, the compositions of the phases changed, particle sizes increased, energy band gaps decreased and electrical conductivity increased. The photoconductivity of thin film was revealed by J-V measurements and slightly increased by annealing. From temperature-dependent J-V measurements, activation energies (E_a) were calculated in low and high temperature regions and, found to be 0.03 eV for low temperature region and 0.8 eV for high temperature one.

Key words: Thin films, InSe, J-V measurements, M-CBD, XRD, AFM

1. Introduction

Indium selenide (In_xSe_y) thin films that can be constructed with various atomic combinations and phases such as InSe, In_2Se_3 , In_4Se_3 , $\text{In}_9\text{Se}_{11}$, In_6Se_7 , etc. have been verified as intriguing inorganic semiconductors during past few decades [1–6]. They attract particular interest of researchers owing to demonstrate noteworthy optical and photophysical properties that are promising for solar cells, photovoltaics, capacitors, microbatteries, field-effect transistors, strain engineering, nonlinear optics and miscellaneous nanoelectronic applications [7–13]. Not only their inherent polymorphism gives opportunity to be utilized as different layers for different purposes depending on the change of extent of band gap but also their junction with diverse substrates and layers enables the fabrication of different devices [1,2,5,14–18]. Especially, the absence or low density of dangling bonds at Van der Waals surfaces of In_xSe_y make them peculiar for heterojunction processing [1,6,19,20]. However, coexistence of different phases in one layer and, presence of unproportional stoichiometries arising from loss of selenium during preparation can be major drawback of In_xSe_y in order to achieve stoichiometric final product [4,20,21]. In many of techniques which were developed for efficient growing of semiconducting thin films on substrates, modified chemical bath deposition method (M-CBD) as modified version of chemical bath deposition (CBD) method is still one of the most appropriate techniques for In_xSe_y growth to alleviate aforementioned handicaps [17,22–24]. It is relatively cheap, easy to apply and straightforward method aside from its advantages such as avoiding waste of materials adjusting rinsing time requiring none of restriction for substrate material, not inducing local overheat, etc. [17,23,24]. Therefore, we rationally benefited from M-CBD method in our study to grow In_xSe_y phase on glass substrate. Optical, photoelectric, compositional and morphological features of the films were analyzed by XRD, AFM, UV-Vis and I-V characterization measurements. Thereby it is aimed to report an alternative for InSe based electronic devices (diode, photodetector, etc.) by varying molarity and annealing temperature parameters.

2. Methods

InSe thin films were deposited at room temperature on glass substrate of $30 \times 26 \times 2$ mm dimensions by M-CBD method. The glass substrates were first boiled in chromic acid, then washed with hydrochloric acid followed by detergent water, and

* Correspondence: fatih.unal@giresun.edu.tr

finally cleaned with acetone and distilled water. For cationic solutions, acidic (pH≈3) $\text{In}_2(\text{SO}_4)_3$ solutions of different molar concentrations were used while for anionic ones, basic (pH≈12) Na_2SeSO_3 solution of 0.05 M was used. Optical properties were investigated using different molar concentrations of cationic precursor solutions while other measurements were made by using 0.07 M cationic precursor solution.

The substrates were 75 times immersed in $\text{In}_2(\text{SO}_4)_3$ precursor solution for 30 s, in distilled water for 70 s, in Na_2SeSO_3 precursor solution for 10 s and distilled water for 70 s respectively, (Figures1 [17] and 2). The two of the fabricated films were also annealed at 100 and 150 °C temperatures in air atmosphere for 1 h.

Structural analyses of thin films were performed with Rigaku D/Max-2200 XRD device in Ankara General Directorate of Mineral Research and Exploration (Cu-K α radiation, $\lambda = 1.5418 \text{ \AA}$, $2\theta = 10\text{--}70^\circ$). Surface morphologies of the films were probed by PSIAXE-100E model Atomic Force Microscopy (AFM). The thickness of the films were calculated using the equation $t = m / \rho_s A$ where t is thickness, m is the mass deposited on substrate, ρ_s is density and A is surface area of deposited film. Optical properties were investigated by Perkin-Elmer Lambda 25 UV-Vis spectrophotometer. The I-V measurements were carried out with Keithley 6486 pico-amperemeter and Pasco Scientific SF-9585. A power source using two probe technique in which silver metal was used for contacts.

3. Results and discussion

3.1. Structural properties

3.1.1. XRD measurements

The thickness of thin film growth on glass substrate in 75 steps was estimated to be 112 nm. Lattice parameters and percentage compositions of phases are given in Table 1. The XRD spectra of thin films were depicted in Figure 3.

Polycrystal composition of In_xSe_y film is understood from the presence of InSe , In_2Se_3 and In_6Se_7 phases in accordance with the previous literature [17] and the ratios of these phases change with annealing. The sharpest peaks for $\text{InSe}(002)$, $\text{In}_2\text{Se}_3(108)$ and $\text{In}_6\text{Se}_7(204)$ phases are observed at $2\theta \approx 39^\circ$, $2\theta \approx 35^\circ$ and $2\theta \approx 23^\circ$, respectively. The particle size (D), dislocation density (δ) and microstrain (ϵ) were calculated in these planes.

D can be calculated according to following Scherrer equation. Some important structural data are given in Table 2.

$$D = \frac{0.90 \cdot \lambda}{\beta \cdot \cos\theta} \tag{1}$$

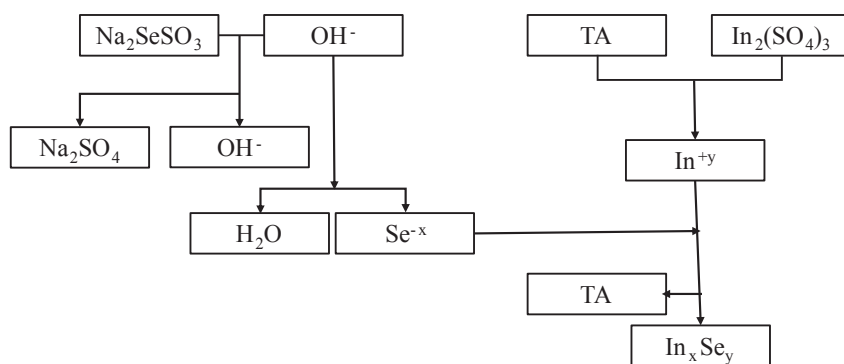


Figure 1. The growing scheme of In_xSe_y thin films (TA: tartaric acid).

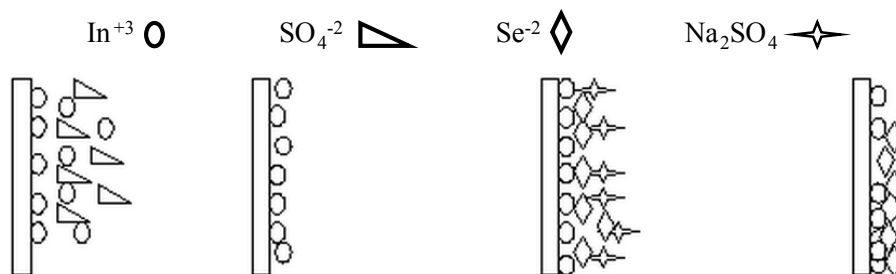


Figure 2. The formation of In_xSe_y thin films by M-CBD method.

Table 1. Lattice parameters of the phases that constituting thin film.

Formula			
	InSe	In ₂ Se ₃	In ₆ Se ₇
Temperature (K)	300		
Ref. No (COD)	96-154-0842	96-152-8775	96-210-6209
Wavelength (Å)	1.5418 (Cu-Kα)		
Crystal system	Monoclinic	trigonal (hexagonal axes)	Monoclinic
Space group	P 1 2/m 1 (10)	R -3 m (166)	P 1 21 1(4)
Unit cell dimensions (Å)			
<i>a</i>	11.020	4.05	9.430
<i>b</i>	4.110	-	4.063
<i>c</i>	4.610	29.410	18.378
<i>B</i> (°)	87.200	-	109.340
Cell volume (Å ³)	208.54	417.76	664.40
<i>Z</i>	6	6	2
	Composition (%)		
As-deposited	25.2	21.2	53.6
100 °C-annealed	28.9	37.9	33.1
150 °C-annealed	27.4	29.6	43.0

Lattice parameters and compositions were calculated using Match! program.

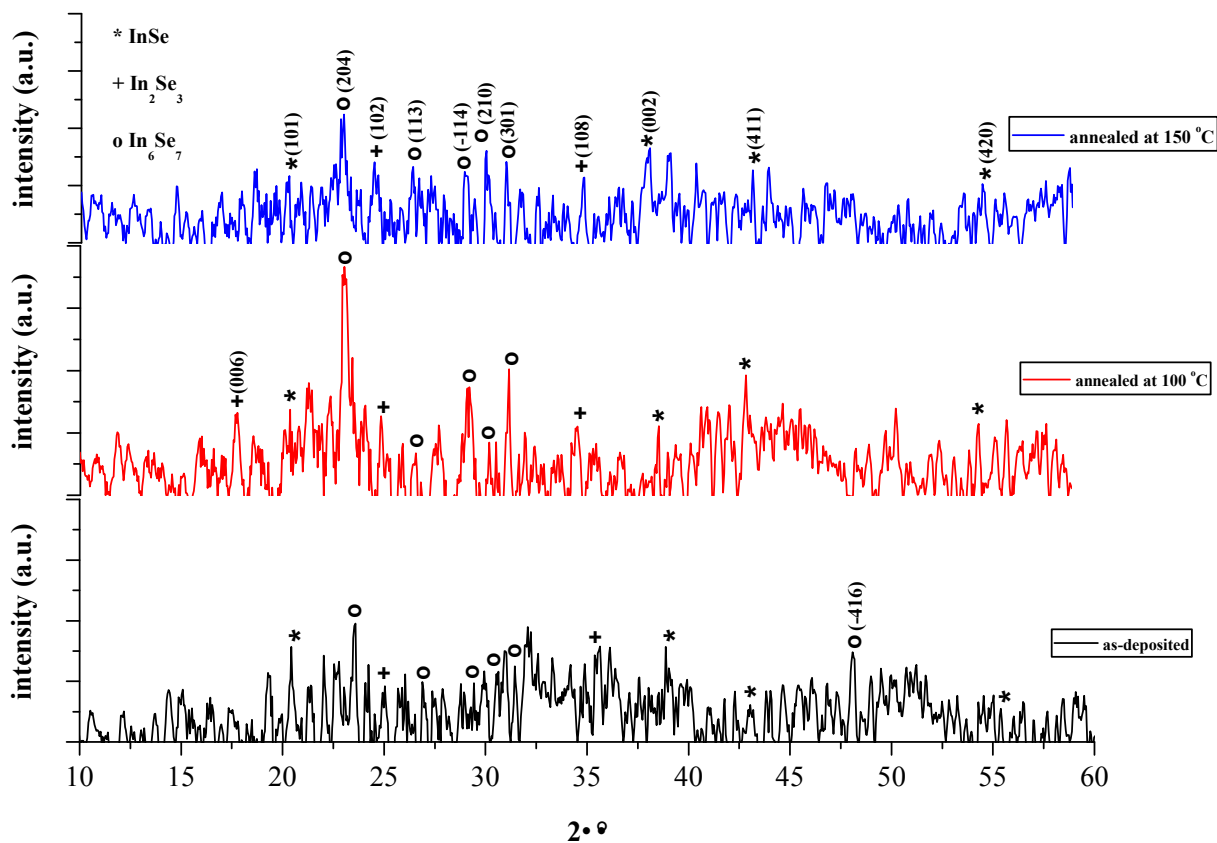


Figure 3. XRD spectra of the as-deposited and annealed thin films obtained from 0.07 M cationic precursor solution.

Table 2. Some important structural parameters of the films.

2θ	Condition	Phase	(hkl)	FWHM (β)	Particle size (D) (nm)	Lattice strain (ε)	Dislocation density (δ) × 10 ¹⁵
23.52703	As-deposited	In ₆ Se ₇	204	0.20655	37.66379905	0.050552979	0.705
35.54204		In ₂ Se ₃	108	0.33524	22.5724337	0.079810913	1.963
38.51931		InSe	002	0.33308	22.52198203	0.078609665	1.971
23.39656	Annealed-100°C	In ₆ Se ₇	204	0.38039	20.45610342	0.09312222	2.389
35.06916		In ₂ Se ₃	108	0.26774	28.3003165	0.063824885	1.248
39.14171		InSe	002	0.1634	45.82175503	0.038490012	0.476
23.2444	Annealed-150°C	In ₆ Se ₇	204	0.11952	65.12240399	0.029267378	0.236
35.35063		In ₂ Se ₃	108	0.12022	62.97806785	0.028636175	0.252
39.11148		InSe	002	0.11533	64.92653007	0.027169335	0.237

where D is particle size, λ is the wavelength of X-rays (1.5406 Å for CuKα), β is the full width at half maximum and θ is Bragg angle.

δ is calculated from Williamson and Smallman's formula

$$\delta = \frac{1}{D^2} \text{ lines/m}^2 \tag{2}$$

ε is obtained using the relation

$$\epsilon = \frac{\beta \cdot \cos\theta}{4} \tag{3}$$

Generally, with annealing, particle size increases while dislocation density and lattice strain decreases (Table 2). The low dislocation density and lattice strain, and high particle size mean that the fine crystallization of film [25, 26].

3.1.2. Surface morphology analyses

From AFM analyses, although clusters took place in some areas, it is observed that the film was growth on glass substrate in homogenous form in which none of cracks formed. Figure 4 represents AFM images of as-deposited, 100 °C-annealed and 150 °C-annealed thin films prepared from 0.07 M cationic precursor solutions. The particle sizes of thin films as-deposited, 100 °C-annealed and 150 °C-annealed were calculated to be 49.2 nm, 69.7 nm, and 106.8 nm, respectively. It is observed that the dimensions of thin films increased with the increase of annealing temperature as well as it is confirmed from XRD analyses. The growing of particle dimensions arises from the accumulation of smaller particles with thermal effect to form bigger ones. This situation is consistent with literature [20,27]. The increase of particle size also gives rise to noticeable increase of peak intensities, which means the increase of crystallization.

3.2. Optical properties

The optical absorption spectroscopy is one of the most used techniques to assign the energy band gap. The relation between absorption coefficient and energy band gap (E_g) is given [28]

$$\alpha(h\nu) \approx (h\nu - E_g)^n \tag{4}$$

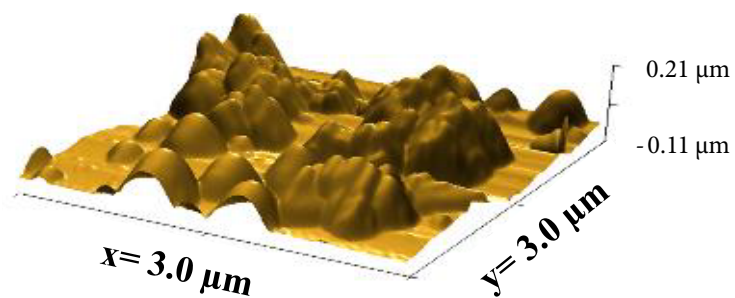
where α is the absorption coefficient, $h\nu$ is energy of photon and E_g is energy band gap. The value of n is ½ for direct allowed transitions for InSe [29] materials. This technique plots $(\alpha h\nu)^{\frac{1}{n}}$ versus $h\nu$. E_g is assigned by extrapolating the straight line portion of the plot to the energy axis. The intercept gives the value of energy band gap.

The relation between absorbance (A) and transmittance (T) is given by

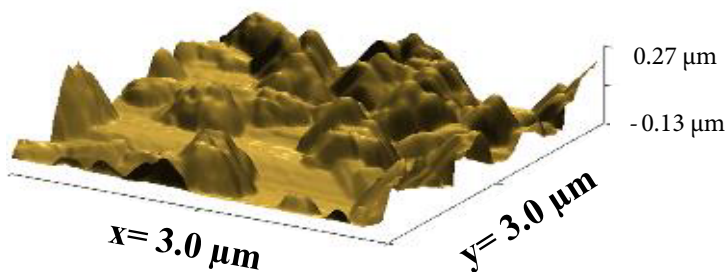
$$A = -\log T \tag{5}$$

and the reflection (R) is given by

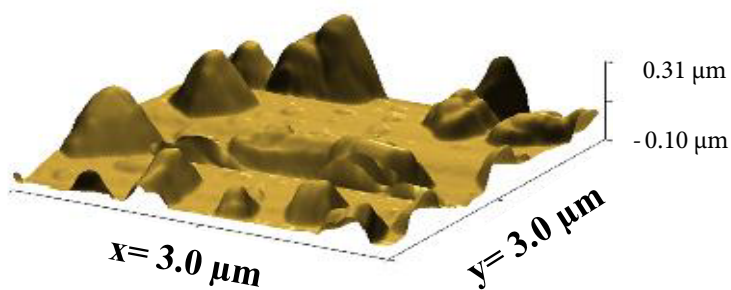
$$R = 1 - (A + T) \tag{6}$$



(a)



(b)



(c)

Figure 4. AFM images of thin films (a: as-deposited, b: 100 °C-annealed, c: 150 °C-annealed).

Then the refractive index (n) is given as [30, 31]

$$n = \frac{1 + \sqrt{R}}{1 - \sqrt{R}} \quad (7)$$

The relation between absorption coefficient (α) and extinction coefficient (k) is given by

$$k = \frac{\lambda \cdot \alpha}{4\pi} \quad (8)$$

where α is calculated from the formula

$$\alpha = \frac{2.303 \cdot A}{d} \quad (9)$$

where d is thickness. The plots of $T(\%)$ vs. λ , band gap vs. $h\nu$, k and n vs. λ of as-deposited and annealed thin films prepared from various molar concentrations of cationic precursor solutions were measured and depicted in Figures 5a–5d, 6a–6d, and 7a–7d, respectively.

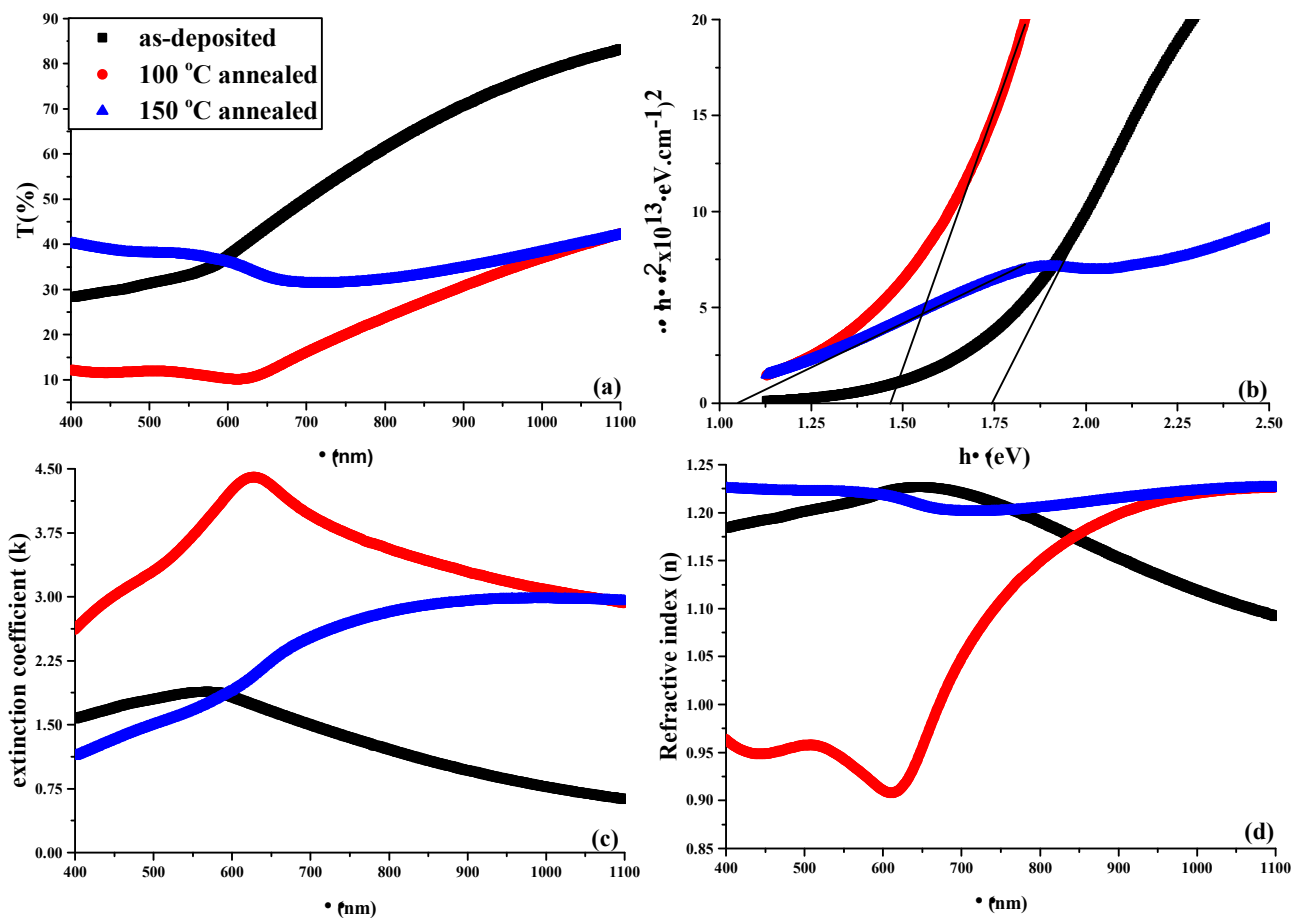


Figure 5. (a) Transmittances, (b) band gaps, (c) extinction coefficients, and (d) refractive indexes of the films obtained from 0.03 M precursor cationic solutions.

Table 3. Transmittance parameters of thin films.

λ (nm)	Transmittance (T)		
	As-deposited	As-deposited	150 °C-annealed
0.03 M			
700	50.02649	50.02649	31.31843
400	28.22279	28.22279	40.2161
0.05 M			
700	34.87386	34.87386	14.75367
400	19.13375	19.13375	25.31629
0.07 M			
700	37.60971	37.60971	29.43744
400	15.03488	15.03488	36.57632

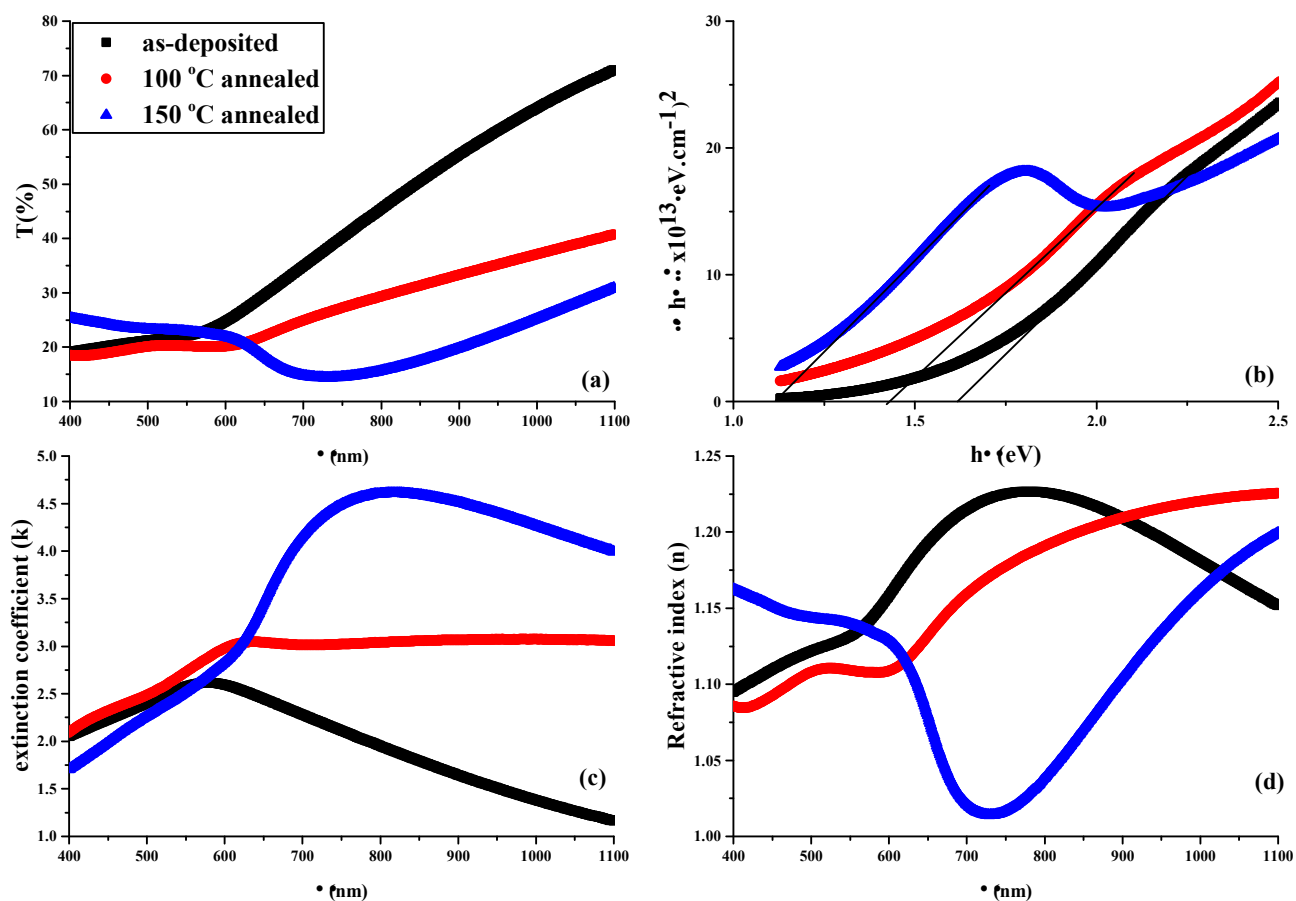


Figure 6. (a) Transmittances, (b) band gaps, (c) extinction coefficients, and (d) refractive indexes of the films obtained from 0.05 M precursor cationic solution.

For visible region limit values, transmittance parameters were given in Table 3 while k and n values were given in Table 4.

In transmittance spectra of thin films, the highest transmittances were observed for as-deposited thin film among all thin films from 1100 to 600 nm while the lowest ones observed for 100 °C-annealed, 150 °C-annealed and 100 °C-annealed thin films from 0.03 M, 0.05 M and 0.07 M cationic precursor solutions, respectively. Within 400–600 nm range 150 °C-annealed thin films exhibit the highest transmittance while 100 °C-annealed thin films exhibit the lowest one among all thin films. Although reasonably low thickness of thin films, the low transmittance of fabricated thin films within visible region boundaries indicate that the fabricated thin films are convenient for devices running in visible region. The changes in molarities of cationic precursor solutions and annealing did not give rise to any trend in k and n values while the change in wavelengths give rise to trend in these values. For all cationic precursor solutions, k values in as-deposited films increased from 1100 nm to around 600 nm and decreased from around 600 nm to 400 nm. In 100 °C-annealed films, for 0.03 M precursor solution, k value increased from 1100 nm to around 640 nm and sharply decreased from around 640 nm to 400 nm while for 0.05 and 0.07 M precursor solutions, k values were almost constant from 1100 nm to 640 nm and sharply decreased again from 640 nm to 400 nm. In 150 °C-annealed films, for all solutions, k values were constant from 1100 nm to around 700 nm and sharply decreased from around 700 nm to 400 nm. In case of n values, in as-deposited film, for 0.03 M precursor solution, n values increased from 1100 nm to 650 nm and decreased from 650 nm to 400 nm. For 0.05 M and 0.07 M precursor solutions, n values increased from 1100 nm to 750 nm and decreased from 750 nm to 400 nm. In 100 °C-annealed films, for 0.03 M precursor solution, n values sharply decreased from 1100 nm to 620 nm and increased from 620 nm to 400 nm. For 0.05 M precursor solution, n values decreased from 1100 nm to 600 nm, slightly increased from 600 nm to 500 nm, and decreased again from 500 nm to 400 nm. For 0.07 M precursor solution, n values decreased from 1100 nm to 630 nm, increased from 630 nm to 500 nm and stayed constant from 500 nm to 400 nm. In 150 °C-annealed films, for 0.03 M and 0.07 M precursor solutions, not a significant change was observed from 1100 nm to 400 nm. For 0.05 M precursor solution, n values sharply decreased from 1100 nm to 730 nm, increased from 730 nm to

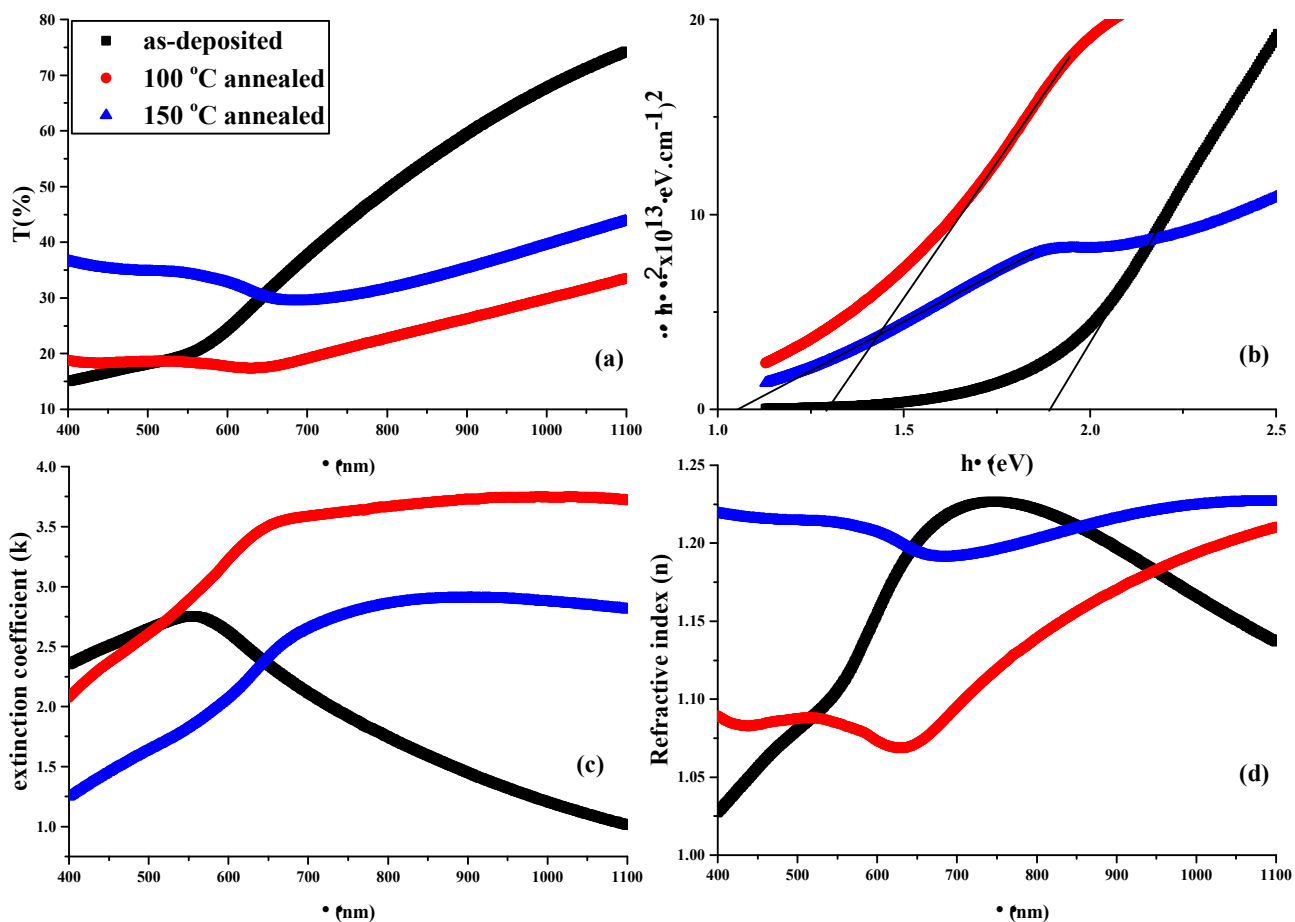


Figure 7. (a) Transmittances, (b) band gaps, (c) extinction coefficients, and (d) refractive indexes of the films obtained from 0.07 M precursor cationic solutions.

Table 4. Extinction coefficients and refractive indexes of the films.

λ (nm)	Extinction coefficients (k)			Refractive indexes (n)		
	As-deposited	100 °C-annealed	150 °C-annealed	As-deposited	100 °C-annealed	150 °C-annealed
0.03 M						
700	1.49764	3.9564	2.51921	1.22072	1.04767	1.20093
400	1.56829	2.61362	1.12926	1.18385	0.96362	1.22499
0.05 M						
700	2.27943	3.01226	4.15622	1.21484	1.15929	1.02099
400	2.05013	2.09153	1.70302	1.09475	1.08577	1.16244
0.07 M						
700	2.11458	3.58624	2.65259	1.22147	1.09493	1.19125
400	2.34901	2.07497	1.24687	1.02711	1.08938	1.21906

600 nm and almost stayed constant from 600 nm to 400 nm. Trends similar to aforementioned were nearly observed in the study reported by Hossain et al. [32].

Table 5 lists the E_g values of the films. The increase of the concentrations of cationic precursor solution inconsistently influences E_g values in as-deposited thin film. However, it is observed that E_g is the function of concentration in 100

Table 5. Assigned energy band gap values.

	Energy band gaps (eV)		
	As-deposited	Annealed at 100 °C	Annealed at 150 °C
Glass/ In _x Se _y 0.03 M C.S	1.73	1.59	1.12
Glass/ In _x Se _y 0.05 M C.S	1.63	1.45	1.16
Glass/ In _x Se _y 0.07 M C.S	1.87	1.3	1.12

C.S: cationic solution.

°C-annealed thin film while it is not reasonably influenced by concentration in 150 °C-annealed film. The reason for these changes probably arises from the change of In:Se stoichiometries. On the other hand, E_g values decreased with annealing. Besides, this can be attributed to several factors: i) particle growth effect, ii) quantum confinement effect, iii) the decrease of dispersions at particle boundaries, iv) the possibility of increase of structural defects, v) phase transitions with annealing treatment [33–35]. The first three of these reasons are also associated with each other.

The quantum confinement effect originating from systematic changes in energy levels as a function of internal dimension influences the particles of around 5 nm or lower sized [33]. As particle size increasing, quantum phenomena become slighter and separations in energy levels become narrower. Consequently, this causes a decrease of E_g. Structural defects cause allowed states at band boundaries in forbidden area and hence decrease E_g.

3.2. Electrical properties

Owing to the lowest transmittance values obtained for 100 °C-annealed film, only current density vs. voltage (J-V) characteristics of 100 °C-annealed thin film were compared with that of as-deposited one. J-V characteristics were investigated in dark and illuminated conditions of 100 W/m² obtained from yellow lamb.

High activation energy values in semiconductors originate from trap states below conduction band or from electronic transitions between valance and conduction bands [36]. Low activation energy values are associated with hopping mechanism of electrons. This mechanism can be explained by weak interactions among donor and acceptor atoms. Impurity scatterings are effective in low temperature region while thermal scatterings are effective in high temperature region [37,38].

Also activation energies for as-deposited film were calculated within 298-428 K temperature range and corresponding logσ-10³/T plots were recorded. The calculations were made according to following equation [39, 40]:

$$\sigma = \sigma_0 \exp(-\Delta E / kT) \tag{10}$$

The schematized representation of fabricated device together with Ag parallel contacts is given in Figure 8. The J-V plots of Ag/ In_xSe_y /Ag and Ag/ In_xSe_y (annealed)/Ag devices were given in Figure 9.

Specific resistance values of as-deposited and annealed thin films are calculated as 1.8 × 10⁸ (ohm-cm) and 1.6 × 10⁸ (ohm-cm), respectively. As inferred from Figure 9, both as-deposited and annealed thin films are sensitive to light. The electrical conductance increases with annealing on account of the increase of particle size, the decrease of energy band gap and the change of distribution of the phases.

With temperature, the conductance of the device increases depending on the decrease of resistance according to J-V plot recorded within 298-428K range in Figure 10. This is a typical behaviour of semiconductor. The logσ-10³/T curve depicted in Figure 11 in this temperature range demonstrates that the activation energy in low temperature region in which doped conductivity is in question is 0.03 eV while the activation energy in high temperature region in which nondoped conductivity is in question is 0.8 eV. The increment in conductance is nonlinear owing to presence of different phases, amorphous structure of the film and formation of clusters on the surface as depicted from AFM images of the film [17]. In Figure 12, temperature dependence of specific resistance is also given. As expected, the specific resistance decreases with increasing temperature.

The fill factors (FF) of both as-deposited and annealed devices were calculated to be according to following equation;

$$FF = \frac{J_{mpp} \cdot V_{mpp}}{J_{sc} \cdot V_{oc}} \tag{11}$$

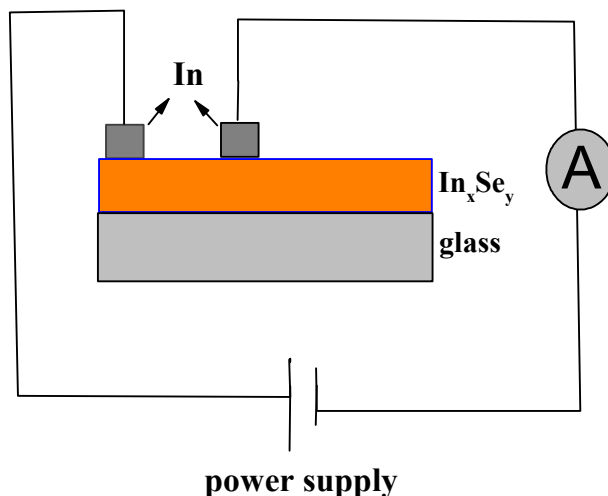


Figure 8. Schematic representation of the fabricated device.

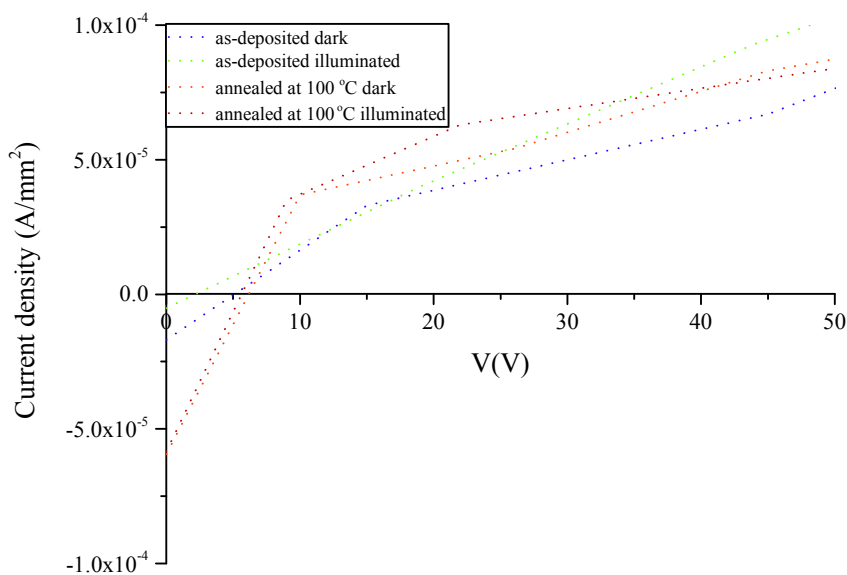


Figure 9. J-V characteristics of $\text{Ag}/\text{In}_x\text{Se}_y/\text{Ag}$ and $\text{Ag}/\text{In}_x\text{Se}_y$ (annealed)/ Ag devices.

where V_{oc} is open circuit voltage, J_{sc} short circuit current, J_{mmp} and V_{mmp} are the current density and voltage at the maximum power point (mmp), respectively.

FF values of the device from as-deposited film in dark and illumination are 0.15 and 0.25 respectively while these of the device from 100 °C-annealed film in dark and illumination are 0.13 and 0.24, respectively.

4. Conclusion

Using M-CBD method as one of the simple, straightforward, cheap and environmental-friendly, In_xSe_y thin films were successfully prepared on the glass substrate. It is revealed that In_xSe_y bears three different phases (InSe , In_2Se_3 , In_6Se_7). With annealing, the composition of the phases changed, particle sizes increased, energy band gaps decreased, electrical conductivities and photoconductivities increased. Concentration-dependence of optical properties using cationic precursor solution (0.03 M, 0.05 M, 0.07 M) was additionally investigated. The lowest transmittance, the lowest n and the highest k in visible region was observed for 0.05 M-150 °C-annealed film. From as-deposited to 100 °C-annealed film, the sharpest narrowing of energy band gap was detected for the film prepared from 0.07 M cationic solution. It is evident from temperature-dependent J-V plots that the film which incorporates mixed phases behave as classical semiconductor with reasonable specific resistance values of 1.8×10^8 (ohm-cm) and 1.6×10^8 (ohm-cm) for as-deposited and 100 °C-annealed

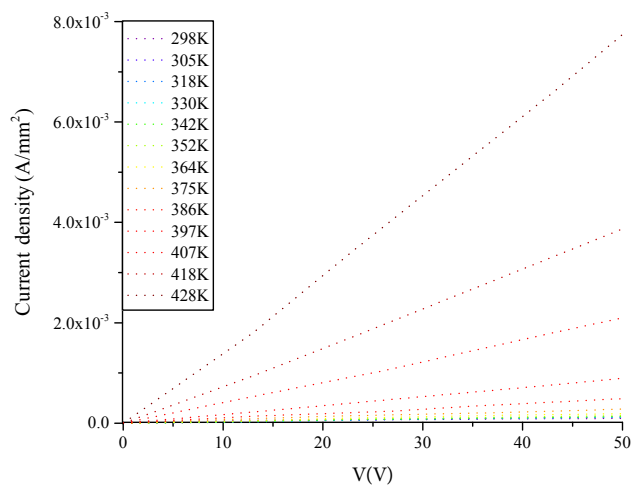


Figure 10. Temperature-dependent J-V characteristics of the as-deposited film.

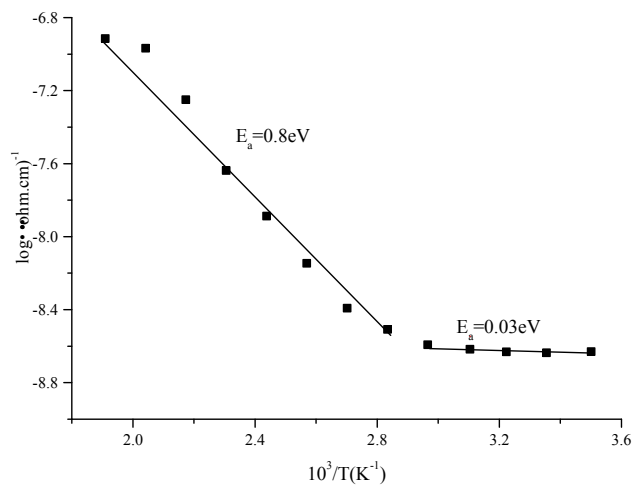


Figure 11. Arrhenius plot of the conductance of thin film ($T =$ absolute temperature).

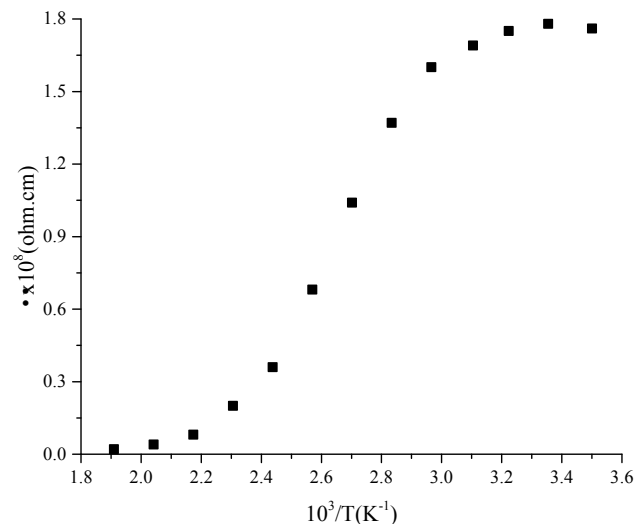


Figure 12. The plots of specific resistance versus $10^3/T$.

films, respectively. Consequently, the lowest transmittance of the film placed around 600–750 nm demonstrates that the prepared film is potential candidate for visible-region photodetectors such as solar cells, photodiodes, etc. In further studies, corresponding properties can be developed by deposition with different semiconductors and heterojunctions.

Contribution of authors Fatih Ünal: Conceptualization, Investigation, Formal analysis, Writing – review and editing. Serkan Demir: Formal analysis, Writing – review and editing. Hasan Mammadov: Investigation, Funding acquisition.

Conflict of interest

The authors declare that they have no known competing financial interests or personal relationships that could have appeared to influence the work reported in this paper.

References

1. Camara MOD, Mauger A, Devos I. Electronic structure of the GaSe/Si(111) and InSe/Si(111) heterojunctions. *Physical Review B covering condensed matter and materials physics* 2002; 65 (20): 205308. doi: 10.1103/PhysRevB.65.205308
2. Camara MOD, Mauger A, Devos I. Electronic structure of the layer compounds GaSe and InSe in a tight-binding approach. *Physical Review B covering condensed matter and materials physics* 2002; 65 (12): 125206. doi: 10.1103/PhysRevB.65.125206
3. Gopal S, Viswanathan C, Thamilselvan M, Premnazeer K, Narayandass SK et al. Conduction studies on electrodeposited indium selenide thin films. *Ionics* 2004; 10 (3-4): 300-303. doi: 10.1007/BF02382835
4. Igasaki Y, Fujiwara T. The preparation of highly oriented InSe films by electrodeposition. *Journal of Crystal Growth* 1996; 158 (3): 268-275. doi: 10.1016/0022-0248(95)00431-9
5. Hirohata A, Moodera JS, Berera GP. Structural and electrical properties of InSe polycrystalline films and diode fabrication. *Thin Solid Films* 2006; 510 (1-2): 247-250. doi: 10.1016/j.tsf.2005.12.202
6. Yandong M, Ying D, Lin Y, Chengwang N, Baibiao H. Engineering a topological phase transition in beta-InSe via strain. *New Journal of Physics* 2013; 15: 073008. doi: 10.1088/1367-2630/15/7/073008
7. Garry WM, Simon AS, Tianhang R, Amalia P, Oleg M et al. Tuning the bandgap of exfoliated InSe Nanosheets by quantum confinement. *Advanced Materials* 2013; 25 (40): 5714-5718. doi: 10.1002/adma.201302616
8. Han G, Chen ZG, Drennan J, Zou J. Indium selenides: structural characteristics, synthesis and their thermoelectric performances. *Small* 2014; 10 (14): 2747-2765. doi: 10.1002/smll.201400104
9. Yükses M, Yaglioglu HG, Elmali A, Aydın EM, Kürüm U et al. Nonlinear and saturable absorption characteristics of Ho doped InSe crystals. *Optics Communications* 2014; 310: 100-103. doi: 10.1016/j.optcom.2013.07.078.
10. Ho CH, Chu YJ. Bending Photoluminescence and Surface Photovoltaic Effect on Multilayer InSe 2D Microplate Crystals. *Advanced Optical Materials* 2015; 3(12): 1750-1758. doi: 10.1002/adom.201500390
11. Boukhalov DW, Gürbulak B, Duman S, Wang L, Politano A et al. The advent of indium selenide: synthesis, electronic properties, ambient stability and applications. *Nanomaterials* 2017; 7 (11): 372. doi: 10.3390/nano7110372
12. Politano A, Campi D, Cattelan M, Amara IB, Jajiri S et al. Indium selenide: an insight into electronic band structure and surface excitations. *Scientific Reports* 2017; 7: 3445. doi: 10.1038/s41598-017-03186-x
13. Zhou J, Shi J, Zeng Q, Chen Y, Niu L et al. InSe monolayer: synthesis, structure and ultra-high second-harmonic generation. *2d Materials* 2018; 5 (2): 025019. doi: 10.1088/2053-1583/aab390
14. Sen SS, Biswas NN, Khan KA. Temperature effect on the electrical and optical properties of indium-selenide thin-films. *Applied Energy* 2000; 65 (1-4): 51-58. doi: 10.1016/S0306-2619(99)00059-8
15. Bouzouita H, Bouguila N, Duchemin S, Fiechter S, Dhoub A. Preparation and characterization of In₂Se₃ thin films. *Renewable Energy* 2002; 25 (1): 131-138. doi: 10.1016/S0960-1481(00)00193-2
16. El-Sayed SM. Optical investigations of the indium selenide glasses. *Vacuum* 2003; 72 (2): 169-175. doi: 10.1016/S0042-207X(03)00139-8
17. Pathan HM, Kulkarni SS, Mane RS, Lokhande CD. Preparation and characterization of indium selenide thin films from a chemical route. *Materials Chemistry and Physics* 2005; 93 (1): 16-20. doi: 10.1016/j.matchemphys.2005.01.063
18. Ornelas RE, Avellaneda D, Shaji S, Castillo GA, Das Roy TK et al. In₆Se₇ thin films by heating thermally evaporated indium and chemical bath deposited selenium multilayers. *Applied Surface Science* 2012; 258 (15): 5753-5758. doi: 10.1016/j.apsusc.2012.02.084
19. Lang O, Klein A, Schlaf R, Löher T, Pettenkofer C et al. InSe/GaSe Heterointerfaces Prepared by Van-Der-Waals Epitaxy. *Journal of Crystal Growth* 1995; 146 (1-4): 439-443. doi: 10.1016/0022-0248(94)00504-4

20. Madugu ML, Bowen L, Echendu OK. Preparation of indium selenide thin film by electrochemical technique. *Journal of Materials Science-Materials in Electronics* 2014; 25 (9): 3977-3983. doi: 10.1007/s10854-014-2116-7
21. Kobbi B, Ouadjaout D, Kesri N. Growth and characterization of In-Se films. *Vacuum* 2001; 62 (4): 321-324. doi: 10.1016/S0042-207X(01)00157-9
22. Lokhande CD, Pathan HM, Giersig M, Tributsch H. Preparation of Zn-x(O,S)(y) thin films using modified chemical bath deposition method. *Applied Surface Science* 2002; 187 (1-2): 101-107. doi: 10.1016/S0169-4332(01)00818-2
23. Pathan HM, Lokhande CD. Deposition of metal chalcogenide thin films by successive ionic layer adsorption and reaction (SILAR) method. *Bulletin of Materials Science* 2004; 27 (2): 85-111. doi: 10.1007/BF02708491
24. Patil RS, Lokhande CD, Mane RS, Pathan HM, Oh-Shim J et al. Successive ionic layer adsorption and reaction (SILAR) trend for nanocrystalline mercury sulfide thin films growth. *Materials Science and Engineering B-Solid State Materials for Advanced Technology* 2006; 129 (1-3): 59-63. doi: 10.1016/j.mseb.2005.12.027
25. Cullity BD. *Elements of X-Ray Diffraction* 2nd Edition. Addison-Wesley Publishing Company Inc. Phillipines: 1978.
26. Zhao Z, Morel DL, Ferekides CS. Electrical and optical properties of tin-doped CdO films deposited by atmospheric metalorganic chemical vapor deposition. *Thin Solid Films* 2002; 413 (1): 203-211. doi: 10.1016/S0040-6090(02)00344-9
27. Lee S, Lee ES, Kim TY, Cho JS, Eo YJ et al. Effect of annealing treatment on CdS/CIGS thin film solar cells depending on different CdS deposition temperatures. *Solar Energy Materials and Solar Cells* 2015; 141: 299-308. doi: 10.1016/j.solmat.2015.05.052
28. Tauc J. Optical properties and electronic structure of amorphous Ge and Si. *Materials Research Bulletin* 1968; 3 (1): 37-46. doi: 10.1016/0025-5408(68)90023-8
29. Gopal S, Viswanathan C, Karunakaran B, Narayandass SK, Mangalaraj D et al. Preparation and characterization of electrodeposited indium selenide thin films. *Crystal Research and Technology* 2005; 40 (6): 557-562. doi: 10.1002/crat.200410383
30. Fadel M, Fayek SA, Abou-Helal MO, Ibrahim MM, Shakra AM. Structural and optical properties of SeGe and SeGeX (X=In, Sb and Bi) amorphous films. *Journal of Alloys and Compounds* 2009; 485 (1): 604-609. doi: 10.1016/j.jallcom.2009.06.057
31. Manificier JC, Gasiot J, Fillard JP. A simple method for the determination of the optical constants n, k and the thickness of a weakly absorbing thin film. *Journal of Physics E: Scientific Instruments* 1976; 9 (11): 1002-1004. doi: 10.1088/0022-3735/9/11/032
32. Hossain J, Julkarnain M, Sharif KS, Khan KA. Optical properties of e-beam evaporated indium selenide (InSe) thin films. *Journal of Scientific Research and Reports* 2014; 3 (12): 1642-1655. doi: 10.9734/JSRR/2014/7658
33. Sahu SN. Preparation, structure, composition, optical and photoelectrochemical properties of vacuum annealed In-Se thin films. *Thin Solid Films* 1995; 261 (1): 98-106. doi: 10.1016/S0040-6090(95)06519-9
34. Matheswaran P, Kumar RS, Sathyamoorthy R. Effect of annealing on the structural and optical properties of InSe bilayer thin films. *Vacuum* 2011; 85 (8): 820-826. doi: 10.1016/j.vacuum.2010.12.004
35. Ateş A, Kundakçı M, Astam A, Yıldırım M. Annealing and light effect on optical and electrical properties of evaporated indium selenide thin films. *Physica E: Low-dimensional Systems and Nanostructures* 2008; 40 (8): 2709-2713. doi: 10.1016/j.physe.2007.12.010
36. Dağdelen F. Investigation of the electronic properties of metal complex semiconductor schottky diodes. PhD, in Institute of Sciences, Firat University, Elazığ, Turkey, 2004.
37. Ünal F. Determination of the structural, optical and electrical characteristics of InSe/rubrene, CIS/rubrene, CIGS/rubrene, InSe/coronene, CIS/coronene, CIGS/coronene heterojoints growth on ITO glass. PhD, in Department of Physics, Inonu University, Malatya, Turkey, 2021.
38. Yazıcı D. The Physical Properties of Phosphine Metal Complexes. MSc, in Department of Physics, Çukurova University, Adana, Turkey, 2007.
39. Kobbi B, Kesri N. Physico-chemical and electrical properties of InSe films. *Vacuum* 2004; 75 (2): 177-182. doi: 10.1016/j.vacuum.2004.02.003
40. Yılmaz S. Investigation of ionic conductivity and relationship with dopant type in the tetragonal (Bi₂O₃)_{1-x}(In₂O₃)_x binary systems (Ln=Dy, Eu, Sm). *Erciyes University Journal of Institute of Science and Technology* 2008; 24: 212-215.